RSC Advances

ROYAL SOCIETY OF CHEMISTRY

www.rsc.org/advances

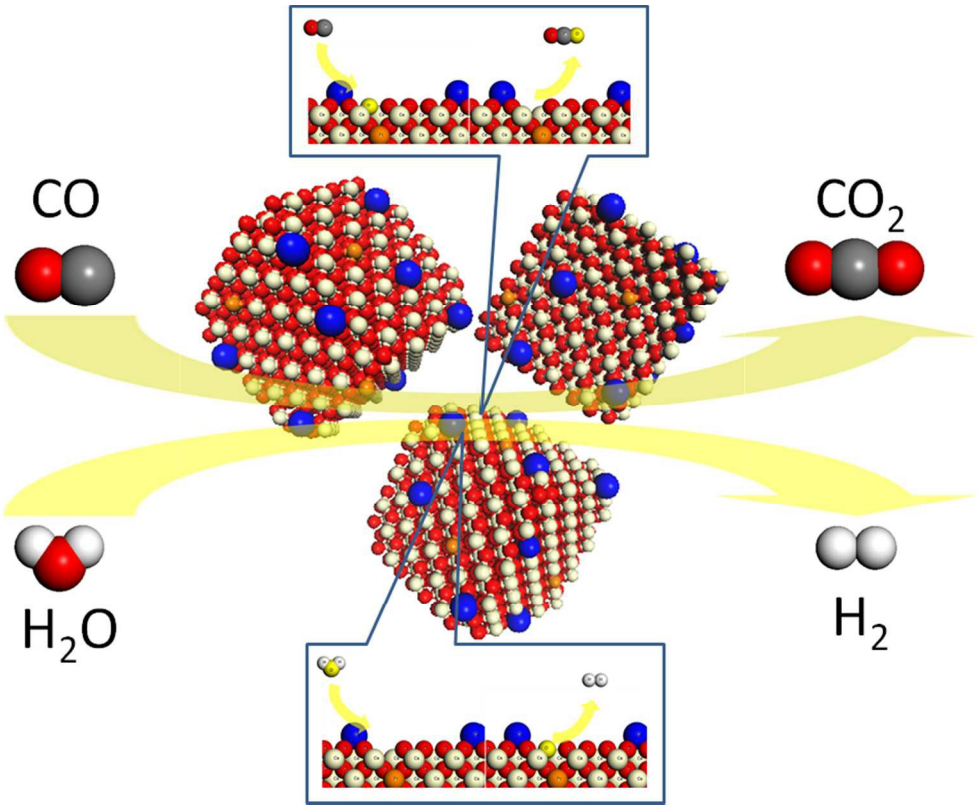

graphical abstract
223x178mm (110 x 110 DPI)

Journal Name

COMMUNICATION

Atomically Dispersed Cu on $Ce_{1-x}RE_xO_{2-\delta}$ nanocubes (RE = La and Pr) for Water Gas Shift: Influence of OSC on Catalysis

Received 00th January 20xx,
Accepted 00th January 20xx

DOI: 10.1039/x0xx00000x

www.rsc.org/

Muhammad Ridwan,[a,c] Rizcky Tamarany,[a] Jonghee Han,[a,b] Suk Woo Nam,[a,b] Hyung Chul Ham, [a,c] Jin Young Kim,[a] Sun Hee Choi,[a] Seong Cheol Jang,[a] and Chang Won Yoon [a,c]*

To elucidate the effect of CeO_2 shape and doping on activity, $Cu_{0.02}Ce_{0.98}O_{2-\delta}$ and $Cu_{0.02}Ce_{0.86}RE_{0.12}O_{2-\delta}$ (RE=La and Pr) were synthesized by a molecular precursor approach. The materials showed distinct activities depending on the shape and composition of CeO_2, which was well correlated with their different oxygen storage capacities.

Owing to intriguing properties, including high oxygen storage capacity (OSC) and oxygen mobility, ceria (CeO_2) has been extensively studied as a metal-oxide support for numerous catalysis reactions.[1-4] In CeO_2-supported catalysts, the OSC of CeO_2 plays a crucial role in catalyzing industrially important reactions, particularly those associated with oxygen ion (O^{2-}) transport, such as water gas shift (WGS) and partial oxidation (POX).[1-4] Significant efforts have been made to improve the OSC to facilitate a number of catalytic reactions. One strategy to enhance the OSC of CeO_2 is through morphology control. CeO_2 nanocubes with (100) facets have increased oxygen vacancies compared with CeO_2 irregular nanoparticles (NPs) with (111) facets.[5] Alternatively, the incorporation of rare earth elements as dopants into the CeO_2 lattice can increase the OSC.[1-4] The doping of CeO_2 with rare earth metal elements such as Pr, La, and Tb increases the OSC, preventing significant carbon coking and ultimately enhancing the catalyst durability in the steam methane reforming reaction.[6] In addition, atomically dispersed metals on oxide supports, Au/M-doped CeO_2 (M = La), were recently reported,[7,8] demonstrating the importance of active site distribution for the WGS reaction and providing an insight into the design of next generation catalysts with highly dispersed active sites.

Herein, we report atomically distributed Cu catalysts supported on La or Pr-doped CeO_2 nanocubes for the WGS reaction. These catalysts were prepared by a molecular precursor method using a Cu-containing organometallic compound. This new synthetic approach for $CuCeREO_{2-\delta}$ (RE = La or Pr) in conjunction with shape control and doping strategies provided the uniformly dispersed active sites with increased OSC needed to achieve high activity for WGS.

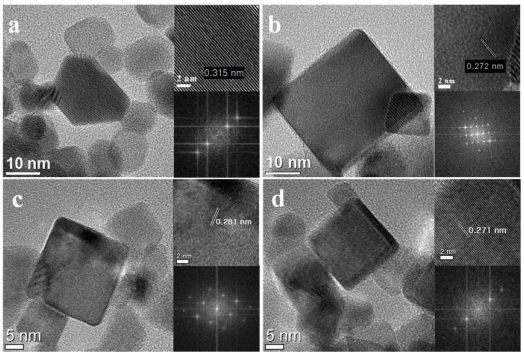

Figure 1. HR-TEM images: (a) CeO_2 irregular NPs (**1**), (b) CeO_2 nanocubes (**2**), (c) $Ce_{0.88}La_{0.12}O_{2-\delta}$ nanocubes (**3**), and (d) $Ce_{0.88}Pr_{0.12}O_{2-\delta}$ nanocubes (**4**).

To improve the OSC of CeO_2, we employed the following synthetic approaches: (i) morphology control and (ii) doping with rare earth elements. Method (i) yielded CeO_2 irregular nanoparticles (NPs) (**1**) and CeO_2 nanocubes (**2**), whereas method (ii) gave $Ce_{0.88}La_{0.12}O_{2-\delta}$ (**3**) and $Ce_{0.88}Pr_{0.12}O_{2-\delta}$ (**4**) nanocubes (*vide infra*). To analyze the shape of the prepared CeO_2 supports, morphological studies of **1** and **2** were conducted by HR-TEM. **1**, prepared by the co-precipitation method, showed irregular shapes with d-spacing of 0.315 nm (Figure 1a), indicating the formation of CeO_2 (111) planes at the surface.[9] In contrast, **2**, obtained by the hydrothermal method, exhibited well-defined cubic structures with uniform sizes of 20–40 nm. The HR-TEM image of **2** shows apparent (100) lattice fringes with an interplanar spacing of 0.272 nm (Figure 1b), suggesting that CeO_2 (100) fringes are dominant at the surface of **2**.[9] Structure determination for **3** and **4** by TEM indicated that doping of La or Pr into **2** did not affect the shape (Figures 1c and 1d).

[a] *Fuel Cell Research Center, Korea Institute of Science and Technology, Seoul 02792, Republic of Korea. E-mail: cwyoon@kist.re.kr; cw.yoon@ust.ac.kr.*
[b] *Korea University, Seoul 02841, Republic of Korea.*
[c] *Clean Energy and Chemical Engineering, Korea University of Science and Technology, Daejeon 34113, Republic of Korea.*

† Footnotes relating to the title and/or authors should appear here.
Electronic Supplementary Information (ESI) available: Materials and detailed preparation procedures, catalyst characterization, catalytic reaction, analysis of products, and DFT calculations. See DOI: 10.1039/x0xx00000x

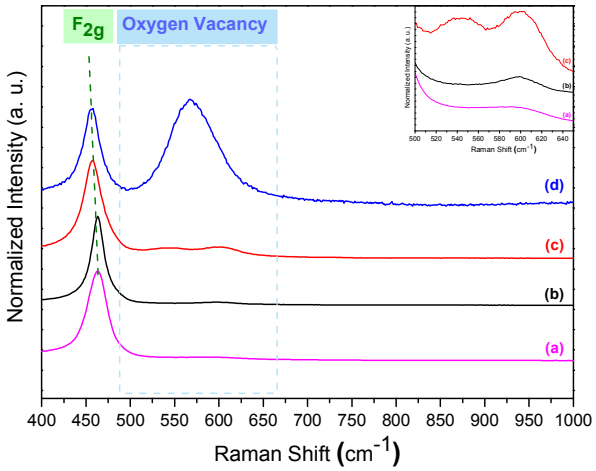

Figure 2. Raman spectra: (a) CeO_2 irregular NPs (**1**), (b) CeO_2 nanocubes (**2**), (c) $Ce_{0.88}La_{0.12}O_{2-\delta}$ nanocubes (**3**), and (d) $Ce_{0.88}Pr_{0.12}O_{2-\delta}$ nanocubes (**4**). Inset presents Raman spectra of **1**, **2** and **3** with the range of 500 – 650 cm^{-1}.

Materials **1**–**4** likely have different OSCs depending on the morphology or dopant. The relative quantities for oxygen vacancies of **1**–**4** were examined using Raman spectroscopy (Figure 2); the sharp peaks with maxima centered at ca. 465 cm^{-1} were attributed to the F_{2g} mode, characteristic of the CeO_2 fluorite crystal structure.[1] Notably, the F_{2g} peaks for **3** and **4** broadened slightly and shifted toward lower frequencies, indicating the formation of solid solutions upon La or Pr incorporation.[1] In addition to the F_{2g} mode, **4** had a dominant peak centered at ca. 570 cm^{-1} owing to oxygen vacancies generated by doping with a trivalent cation; replacement of Ce^{4+} in the CeO_2 lattice with Pr^{3+} produces an oxygen vacancy to maintain charge neutrality.[3] Likewise, the Raman spectrum of **3** had two additional modes at 540 and 600 cm^{-1} associated with the local vibrations of different oxygen vacancy (VO) complexes.[1] Particularly, the vibrational mode at 600 cm^{-1} originates from the presence of Ce^{3+}–VO complexes in the CeO_2 lattice, referred to as the intrinsic vacancy mode, whereas that of ~540 cm^{-1} comes from extrinsic vacancy mode related to La doping.[10] In the Pr-doped samples the extrinsic vacancy mode appears at ~570 cm^{-1}. A higher I_{575}/I_{465} ratio indicates a higher quantity of oxygen vacancies.[11] These results suggest that among these materials, the ability for the formation of oxygen vacancies for **4** is superior.

We also employed Ce 3d X-ray photoelectron spectroscopy (XPS) to determine the relative capability for oxygen vacancy formation of **1**–**4** by assessing their $Ce^{3+}/[Ce^{3+}+Ce^{4+}]$ ratios. The XPS spectra had seven peaks corresponding to Ce $3d_{3/2}$ (897–915 eV) and Ce $3d_{5/2}$ (875–897 eV)[12] (u and v, respectively, Figure S1). The relative Ce^{3+} $3d_{5/2}$ (v′) / [Ce^{3+} $3d_{5/2}$ (v′) + Ce^{4+} $3d_{5/2}$ (v, v″, and v‴)] ratios for **1**–**4**, determined from the integrated areas of the fitted data (Figure S1, Table S1), provide useful information about the oxygen vacancies. **1** and **2**, which have different shapes, had Ce^{3+} fractions of 15% and 27%, respectively, indicating that **2** has increased oxygen ion mobility compared with **1**. In contrast, the incorporation of La or Pr into **2** to obtain **3** or **4** did not alter the $Ce^{3+}/[Ce^{3+}+Ce^{4+}]$ ratio, consistent with a previous result.[13]

To gain further information about OSC of the materials, we employed thermogravimetric analyses (Figure S2), according to a previously reported method.[5] Since WGS reactions were conducted at < 400 °C (*vide infra*), we determined the quantities of oxygen vacancies using the heating temperature of 400 °C. The catalysts were initially heated from room temperature to 400 °C with air flow. In this process, oxygen vacancies presented in a catalyst were filled by O_2. At 400 °C, N_2 gas was then supplied for 10 min to abstract the filled oxygen from the catalyst, which resulted in weight loss. Repeated the processes gave the quantities of oxygen vacancies in the catalyst (Table 1). Consistent with the Raman results, the measured OSCs were found to increase in the order of **4** > **3** > **2** > **1**.

Table 1. Calculated oxygen vacancies for **1** - **4** based on thermogravimetric analysis at 400 °C.

Samples	Weight loss (%)	μmol of O_2/g_{cat} [a]
CeO_2 irregular NPs (**1**)	0.034	10
CeO_2 nanocubes (**2**)	0.052	16
$Ce_{0.88}La_{0.12}O_{2-\delta}$ nanocubes (**3**)	0.072	22
$Ce_{0.88}Pr_{0.12}O_{2-\delta}$ nanocubes (**4**)	0.074	23

[a] The quantities of oxygen vacancy = g of decreased weight / molecular weight of O_2.[5]

The enhanced OSC of the modified CeO_2 materials could provide catalysts with improved activity. We incorporated Cu into the crystal structure of CeO_2 to generate catalytically active sites for the WGS. Precipitation, wet impregnation, or co-precipitation deposition methods have widely been employed to introduce dopants into metal oxide lattices, but metal aggregates are often formed. Recently, atomically dispersed active sites supported on metal oxides were shown to be highly active for CO oxidation and WGS;[7, 14] the WGS reaction was accelerated by uniformly dispersed, nonmetallic Au or Pt species strongly associated with CeO_2 that generated by removing excess Au or Pt in nanostructured Au- or Pt-CeO_x materials.[7]

We employed a different synthetic strategy using an organometallic precursor, $Cu(OCH_3)_2$, to dope Cu atoms into CeO_2 with increased distribution (Figure 3). The surface hydroxyl (–OH) groups functioned as nucleophiles to react with $Cu(OCH_3)_2$ to yield Cu-anchored CeO_2 and CH_3OH as a byproduct (Figure 3, reactions A and B). A reaction of **2** (0.20 g) with $Cu(OCH_3)_2$ (2.9 mg, 0.023 mmol) at 70 °C for 24 h clearly indicated the formation of CH_3OH, as evidenced by ^1H NMR spectroscopy (Figure S3). Note that Cu agglomeration was likely minimized by the steric hindrance of the organometallic precursor. The well-dispersed Cu atoms were then incorporated into the CeO_2 lattice by calcination at 400 °C (Figure 3, reaction C). In fact, similar surface grafting methods for CeO_2 with organosilanes to improved chemical mechanical polishing.[15, 16] The as-synthesized catalysts are denoted as $Cu_{0.02}Ce_{0.98}O_{2-\delta}$ irregular NPs (**Cu-1**), $Cu_{0.02}Ce_{0.98}O_{2-\delta}$ nanocubes (**Cu-2**), $Cu_{0.02}Ce_{0.86}La_{0.12}O_{2-\delta}$ nanocubes (**Cu-3**), and $Cu_{0.02}Ce_{0.86}Pr_{0.12}O_{2-\delta}$ nanocubes (**Cu-4**). For comparison, $CuCeO_2$ was prepared by a conventional process using $Cu(NO_3)_2$, followed by $NaBH_4$ reduction: $Cu_{0.02}Ce_{0.98}O_{2-\delta}$ irregular NPs (**Cu-5**) and $Cu_{0.02}Ce_{0.98}O_{2-\delta}$ nanocubes (**Cu-6**).

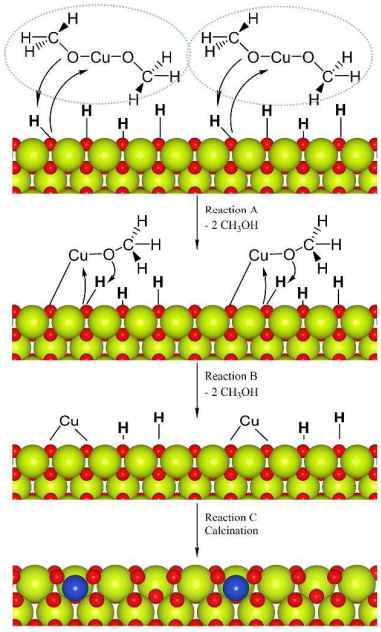

Figure 3. A schematic diagram for the generation of uniformly distributed Cu active sites based on a molecular precursor approach (yellow: Ce atom, red: O atom, and blue: Cu atom).

Table 2. Characterization of the prepared $CuCeO_2$ catalysts.

Catalyst	Cu precursor	Method	Metal loading (wt%)[b]	BET surface area (m^2/g)
Cu-1	$Cu(OCH_3)_2$	Molecular precursor approach	0.70	56
Cu-2	$Cu(OCH_3)_2$		0.58	28
Cu-3	$Cu(OCH_3)_2$		0.62	30
Cu-4	$Cu(OCH_3)_2$		0.61	29
Cu-5	$Cu(NO_3)_2{\cdot}3H_2O$ [a]	Conventional co-reduction	0.70	56
Cu-6	$Cu(NO_3)_2{\cdot}3H_2O$ [a]		0.74	27

[a] Cu reduced using $NaBH_4$. [b] measured by SEM-EDS.

The $CuCeO_2$-based catalysts were characterized using BET and SEM-EDS (Table 2). SEM-EDS indicated that 0.58–0.74 wt% of Cu was deposited on the catalysts. STEM-EDS mapping indicated the presence of well-dispersed Cu in **Cu-2** (as an example, Figure S4). X-ray diffraction analyses of **Cu-1**–**Cu-4** showed only the characteristic peaks of the CeO_2 fluorite cubic structure (Figure S5), indicating that the Cu atoms were well dispersed and formed a Cu-doped CeO_2 solid solution. The low valence state of Cu^{2+}, with its smaller ionic radius, was reported to allow facile substitution of Ce^{4+} in the CeO_2 lattice with simultaneous oxygen vacancy generation to produce a $Cu_xCe_{1-x}O_{2-\delta}$ solid solution.[4]

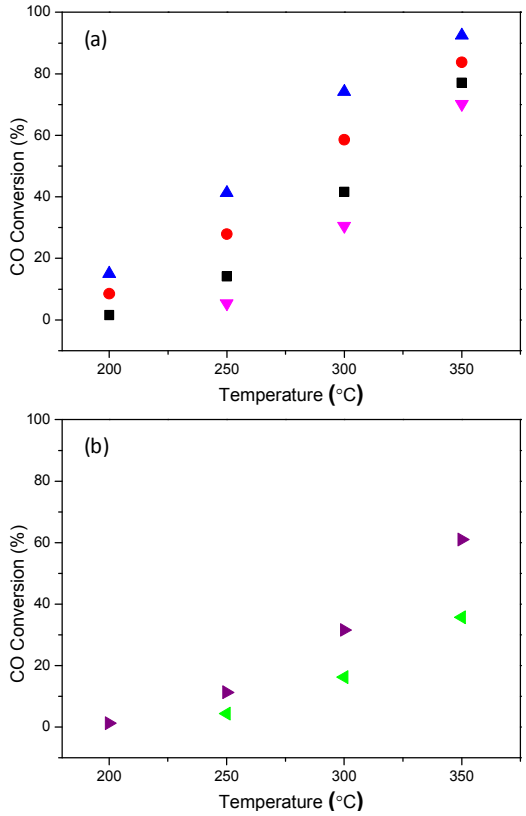

Figure 4. CO conversions during the WGS over the catalysts: (a) **Cu-1** (▼, pink), **Cu-2** (■ black), **Cu-3** (●, red), and **Cu-4** (▲, blue); (b) **Cu-5** (▶, purple) and **Cu-6** (◀, green).

We determined the catalytic activities of **Cu-1**–**Cu-6** for the WGS reactions. First, we verified the influence of CeO_2 facets on the WGS (Figure 4). **Cu-2** is expected to show higher activity than **Cu-1** since the CeO_2 nanocubes have a higher OSC than the CeO_2 irregular NPs owing to the high surface energy of the (100) facet, which originates from the instability of the top layer oxygen atoms that bridge two cerium atoms.[17] Recently, the OSC of CeO_2 was determined using thermogravimetric analysis and, although nanocubes have smaller surface areas than irregular NPs, the OSC of CeO_2 nanocubes was nearly 2.6 times higher than that of CeO_2 irregular NPs at 400 °C.[18] Similarly, the CO conversion using **Cu-2** (42%) was greater than that of **Cu-1** (30%) at 300 °C (Figure 4a). Next, we examined the influence of doping by comparing **Cu-2**, **Cu-3**, and **Cu-4**. Compared with **Cu-2**, **Cu-3** and **Cu-4** had increased activities, presumably owing to the enhanced OSC caused by doping CeO_2 with rare earth elements;[1-4] the CO conversion of **Cu-4** (74%) was 1.8 times higher than that of **Cu-2** at 300 °C. Given the influence of both facet control and doping, **Cu-4** has significantly increased activity (2.5 times higher than that of **Cu-1** at 300 °C); this result correlates well with the relative OSCs of **1**–**4**. In contrast, **Cu-5**, with dominant Cu (111) facets, had a higher catalytic activity than the **Cu-6** nanocubes, with CO conversions of 32% and 16% at 300 °C, respectively (Figure 4b). The CO conversion appears to be linear but it is expected to have a sigmoidal shape in an expanded temperature range. An Arrhenius plot obtained using the temperature dependent kinetic data for **Cu-4** gave an activation energy of 22 kJ/mol, which is considerably lower than that of **Cu-1** (Figure S6 and Table S2). We further conducted DFT calculations to

determine the influence of the dopants on oxygen vacancy formation at the materials. Our calculations strongly support that the Pr-doped CeO_2 likely has the highest oxygen vacancy mobility (Figures S7 and S8).

$$CO + \text{Cu-Ce-(O)-RE} \rightarrow CO_2 + \text{Cu-Ce-( )-RE} \quad (1)$$

$$H_2O + \text{Cu-Ce-( )-RE} \rightarrow H_2 + \text{Cu- Ce-(O)-RE} \quad (2)$$

$$\text{Overall: } CO + H_2O \rightarrow CO_2 + H_2 \quad (3)$$

Based on the experimental results, a plausible mechanism involves oxygen transfer from $CuCeREO_2$. First, CO reacts with oxygen atoms in the CeO_2 surface lattice to generate an oxygen vacancy (Eq. 1). The resulting lattice abstracts an oxygen atom from H_2O to produce hydrogen (Eq. 2). The process is highly dependent on the OSC of the catalyst.

In summary, $CuCeREO_{2-\delta}$ (RE = La or Pr) catalysts were prepared using the molecular precursor approach to generate Cu active sites well dispersed on CeO_2-based supports. These catalysts were superior to those synthesized by the conventional co-reduction method. The catalytic activities for the WGS were enhanced owing to the increased OSC of CeO_2; the catalyst with exposed (100) facets had better activity than that with exposed (111) facets. In addition, the doped materials with CeO_2 (100) facets had even higher catalytic performance than the undoped $CuCeO_2$ material. Our synthetic approach using an organometallic precursor provides insights into the design of new types of catalysts applicable to numerous chemical transformations.

Acknowledgement

The authors thank the Global Research Laboratory (GRL) Program through the National Research Foundation of Korea funded by the Ministry of Science, ICT and Future Planning of Republic of Korea. The part of the research was also supported by the Fundamental Technology Development Programs for the Future through the Korea Institute of Science and Technology as well as by the National Research Foundation of Korea Grant funded by the Korean Government (MSIP) (University-Institute cooperation program). The computational resources were supported by the supercomputing center of Korea Institute of Science and Technology Information (KISTI) (KSC-2015-C2-002).

References

1. J. R. McBride, K. C. Hass, B. D. Poindexter and W. H. Weber, *J. Appl. Phys.*, 1994, **76**, 2435-2441.
2. D. Harshini, Y. Kim, S. Nam, T.-H. Lim, S.-A. Hong and C. Yoon, *Catal. Lett.*, 2013, **143**, 49-57.
3. M. Guo, J. Lu, Y. Wu, Y. Wang and M. Luo, *Langmuir*, 2011, **27**, 3872-3877.
4. D. Zhang, Y. Qian, L. Shi, H. Mai, R. Gao, J. Zhang, W. Yu and W. Cao, *Catal. Commun.*, 2012, **26**, 164-168.
5. J. Zhang, H. Kumagai, K. Yamamura, S. Ohara, S. Takami, A. Morikawa, H. Shinjoh, K. Kaneko, T. Adschiri and A. Suda, *Nano Lett.*, 2011, **11**, 361-364.
6. D. Harshini, D. H. Lee, J. Jeong, Y. Kim, S. W. Nam, H. C. Ham, J. H. Han, T.-H. Lim and C. W. Yoon, *Applied Catalysis B: Environmental*, 2014, **148–149**, 415-423.
7. Q. Fu, H. Saltsburg and M. Flytzani-Stephanopoulos, *Science*, 2003, **301**, 935-938.
8. M. Yang, L. F. Allard and M. Flytzani-Stephanopoulos, *J. Am. Chem. Soc.*, 2013, **135**, 3768-3771.
9. S. Bernal, G. Blanco, J. J. Calvino, C. López-Cartes, J. A. Pérez-Omil, J. M. Gatica, O. Stephan and C. Colliex, *Catal. Lett.*, 2001, **76**, 131-137.
10. Z. D. Dohčević-Mitrović, M. Grujić-Brojčin, M. Šćepanović, Z. V. Popović, S. Bošković, B. Matović, M. Zinkevich and F. Aldinger, *J. Phys.: Condens. Matter*, 2006, **18**, S2061.
11. M.-F. Luo, Z.-L. Yan, L.-Y. Jin and M. He, *The Journal of Physical Chemistry B*, 2006, **110**, 13068-13071.
12. M. A. Henderson, C. L. Perkins, M. H. Engelhard, S. Thevuthasan and C. H. F. Peden, *Surf. Sci.*, 2003, **526**, 1-18.
13. N. Paunovic, Z. Dohcevic-Mitrovic, R. Scurtu, S. Askrabic, M. Prekajski, B. Matovic and Z. V. Popovic, *Nanoscale*, 2012, **4**, 5469-5476.
14. B. Qiao, A. Wang, X. Yang, L. F. Allard, Z. Jiang, Y. Cui, J. Liu, J. Li and T. Zhang, *Nat Chem*, 2011, **3**, 634-641.
15. Z. Zhang, L. Yu, W. Liu and Z. Song, *Appl. Surf. Sci.*, 2010, **256**, 3856-3861.
16. K. Moller and T. Bein, *Chem. Mater.*, 1998, **10**, 2950-2963.
17. H. Nörenberg and J. H. Harding, *Surf. Sci.*, 2001, **477**, 17-24.
18. T. Adschiri, Y. Hakuta, K. Sue and K. Arai, *J. Nanopart. Res.*, 2001, **3**, 227-235.

